

# Lung Nodule Detection With Modern Low-Field MRI (0.55 T) in Comparison to CT

Maximilian Hinsen, Armin M. Nagel, PhD, Matthias S. May, MD, Marco Wiesmueller, MD,  
Michael Uder, MD, and Rafael Heiss, MD, MHBA

Downloaded from http://investigativeradiology.wolterskluwer.com by BrDMSerHkanZoumJNahJLUEZgo on 09/01/2023

**Objectives:** The aim of this study was to evaluate the accuracy of modern low-field magnetic resonance imaging (MRI) for lung nodule detection and to correlate nodule size measurement with computed tomography (CT) as reference.

**Materials and Methods:** Between November 2020 and July 2021, a prospective clinical trial using low-field MRI at 0.55 T was performed in patients with known pulmonary nodules from a single academic medical center. Every patient underwent MRI and CT imaging on the same day. The primary aim was to evaluate the detection accuracy of pulmonary nodules using MRI with transversal periodically rotated overlapping parallel lines with enhanced reconstruction in combination with coronal half-Fourier acquired single-shot turbo spin-echo MRI sequences. The secondary outcome was the correlation of the mean lung nodule diameter with CT as reference according to the Lung Imaging Reporting and Data System. Nonparametric Mann-Whitney *U* test, Spearman rank correlation coefficient, and Bland-Altman analysis were applied to analyze the results.

**Results:** A total of 46 participants (mean age  $\pm$  SD, 66  $\pm$  11 years; 26 women) were included. In a blinded analysis of 964 lung nodules, the detection accuracy was 100% for those  $\geq 6$  mm (126/126), 80% (159/200) for those  $\geq 4$ – $< 6$  mm, and 23% (147/638) for those  $< 4$  mm in MRI compared with reference CT. Spearman correlation coefficient of MRI and CT size measurement was  $r = 0.87$  ( $P < 0.001$ ), and the mean difference was  $0.16 \pm 0.9$  mm.

**Conclusions:** Modern low-field MRI shows excellent accuracy in lesion detection for lung nodules  $\geq 6$  mm and a very strong correlation with CT imaging for size measurement, but could not compete with CT in the detection of small nodules.

**Key Words:** low-field MRI, magnetic resonance imaging, lung imaging, chest MRI, lung nodules, lung cancer, lung neoplasms

(Invest Radiol 2023;00: 00–00)

Lung cancer is the second most common type of cancer in men and women and the most common cause of cancer-related death.<sup>1</sup> Early detection of lung carcinomas and metastases can lead to improved outcomes.<sup>2–4</sup> Computed tomography (CT) is the reference standard for the detection of both lung carcinomas and lung metastases due to its high spatial resolution, fast scan time, and high contrast. Despite these advantages, it is associated with not inconsiderable radiation exposure, especially with repeated examinations. In recent years, lung cancer

screening has been on the rise in several countries, including the United States, Germany, and France, because of the high health care burden of lung cancer, although such screening results in an increase in the population's radiation dose.<sup>2,5–7</sup> Magnetic resonance imaging (MRI) is not only a radiation-free option for lung imaging, but also offers the advantage of advanced soft tissue characterization and could reduce follow-up examinations.<sup>8–10</sup>

Even with these inherent advantages, which have contributed to the continued success of MRI in other body regions such as the central nervous and musculoskeletal systems, lung MRI has not been established in the clinical routine, apart from a few exceptional cases.<sup>11,12</sup> Some reasons for this are the problematic MR physics-related issues, with a large number of air-tissue interfaces, and the longer acquisition time in an area where motion during the examination is unavoidable (heartbeat, breathing). Recent developments in MRI scanners offer improvements in these issues, with modern low-field MRI providing an inherent reduction in susceptibility artifacts in the lung parenchyma.<sup>13–15</sup> Breath-gated image acquisition using modern sequences combined with a state-of-the-art receiver coil system allows high spatial resolution.<sup>16,17</sup> Recent studies presented the potential of these technical improvements in not only diagnostic morphological imaging but also the assessment of lung function.<sup>16–21</sup>

These improvements could also make MRI a powerful tool for radiation-free detection of early-stage lung cancer and other malignant incidental lung lesions.<sup>11,20</sup> According to the recommendations of the American College of Radiology, lesion size and rate of growth remain the critical values in estimating the entity of lung lesions with a mean lesion diameter of  $\geq 6$  mm, which have a risk of malignancy  $\geq 1\%$  and therefore require intensification of the screening intervals.<sup>7,22,23</sup> For MRI to be a potential alternative to CT in lung cancer detection, it must achieve high accuracy for lung nodule detection and an equivalent determination of size compared with CT.

Consequently, this prospective study aims to compare the accuracy of a modern low-field MRI in lung nodule detection to CT as reference and to correlate lung nodule diameter measurements between low-field MRI and CT.

## MATERIALS AND METHODS

### Ethical Approval

This prospective study was approved by the local ethics committee (Friedrich-Alexander-Universität Erlangen-Nürnberg; No 483\_20 B). Written informed consent was obtained from all participants before study inclusion.

### Study Design

Between November 2020 and July 2021, we performed a cross-sectional investigator-initiated trial to investigate the accuracy of modern low-field lung MRI for lung nodule detection at a single academic medical center. We enrolled consecutive patients with known lung nodules scheduled for a CT lung examination at our institution. Inclusion criteria were (1) a medical indication for CT examination of the lung, (2) known lung nodules identified in a previous CT examination

Received for publication April 17, 2023; and accepted for publication, after revision, June 10, 2023.

From the Institute of Radiology, University Hospital Erlangen, Friedrich-Alexander-Universität Erlangen-Nürnberg (FAU), Erlangen, Germany (M.H., A.M.N., M.S.M., M.W., M.U., R.H.); and Division of Medical Physics in Radiology, German Cancer Research Center, Heidelberg, Germany (A.M.N.).

Conflicts of interest and sources of funding: M.U., M.M., and R.H. are part of the speakers bureau of Siemens Healthcare GmbH. The authors have no further affiliation with any organization with a direct or indirect financial interest in the subject matter discussed in the article.

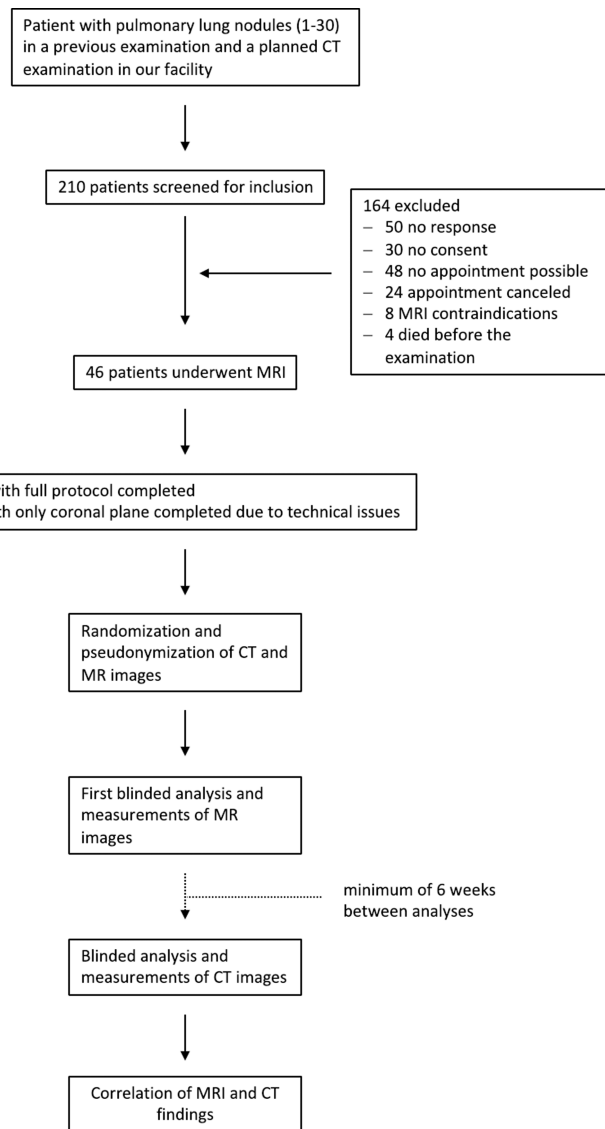
Correspondence to: Rafael Heiss, MD, MHBA, Institute of Radiology, University Hospital Erlangen, Friedrich-Alexander-Universität Erlangen-Nürnberg, Maximiliansplatz 1, 91054 Erlangen, Germany. E-mail: rafael.heiss@uk-erlangen.de.

Supplemental digital contents are available for this article. Direct URL citations appear in the printed text and are provided in the HTML and PDF versions of this article on the journal's Web site ([www.investigativeradiology.com](http://www.investigativeradiology.com)).

Copyright © 2023 Wolters Kluwer Health, Inc. All rights reserved.

ISSN: 0020-9996/23/0000-0000

DOI: 10.1097/RRL.0000000000001006

**FIGURE 1.** Flowchart of the study.

based on the report within the radiological information system, and (3) the ability to give informed consent. Patients were called by a medical doctor in advance for getting their consent for study participation. Exclusion criteria were (1) MRI contraindication (eg, cardiac pacemaker), (2) pregnancy, (3) age younger 18 years, and (4) claustrophobia. Every patient who fulfilled the inclusion criteria was called the week before their CT appointment and asked for voluntary participation in the study. The participants underwent CT imaging for clinical purposes and low-field MRI on the same day.

The first and corresponding authors were responsible for the data collection and site monitoring.

The first author had constant access to the data and performed the statistical analysis and wrote the first draft of the manuscript independent of commercial support.

### Magnetic Resonance Imaging

All low-field MRI examinations were performed at 0.55 T (MAGNETOM Free.Max; Siemens Healthcare GmbH, Erlangen, Germany). Phased-array receiver coils included a 9-channel spine array,

a 12-channel head/neck array, and a 6-channel flex coil. Previous tests showed a more homogeneous signal of the superior thoracic aperture with increased image quality when additionally using the head/neck coil. Two-dimensional turbo spin-echo (TSE) sequences were set up for free-breathing lung MRI in transverse and coronal orientation with a navigator at the liver dome. The gated image acquisition took place during expiration. The transverse image with periodically rotated overlapping parallel lines with enhanced reconstruction (PROPELLER) readout was proton density-weighted (repetition time/echo time, 3000/34 milliseconds) with  $1.1 \times 1.1 \text{ mm}^2$  in-plane resolution, 6-mm slice thickness, a  $336 \times 336$  matrix, GRAPPA as acceleration technique (acceleration factor of 2), and a mean acquisition time of  $8:41 \pm 3:02$  minutes. The coronal image was acquired with a short-tau inversion recovery (STIR) preparation and a half-Fourier acquired single-shot turbo spin-echo (HASTE) readout with T2-weighting (repetition time/echo time, 250/74 milliseconds),  $1.5 \times 1.5 \text{ mm}^2$  in-plane resolution, 6-mm slice thickness, a  $272 \times 272$  matrix, GRAPPA as acceleration technique (acceleration factor of 2), and a mean acquisition time of  $7:58 \pm 3:25$  minutes. For both sequences, participants were set up in a head-first supine position with arms down.

### Computed Tomography

Computed tomography examinations of the chest were acquired in inspiration during clinical routine, using 3 different CT scanners. Most of the scans were performed on 128-slice CT scanners (38 patients on a SOMATOM go.Top and 2 on a SOMATOM X.cite; Siemens Healthcare GmbH, Erlangen, Germany). Six scans were performed on a 384-slice CT scanner (SOMATOM Force; Siemens Healthcare GmbH, Erlangen, Germany). Imaging reconstructions were performed in transversal planes with a slice thickness of 1.0 mm and an increment of 0.7 mm.

### Imaging Evaluation

Reading of both CT and MRI DICOM images was performed at a diagnostic monitor (EIZO RX660, Hakusan, Japan). First, CT and MR images were randomized and pseudonymized by the first author. The blinded data sets were passed to the reader for separate evaluation on a 3D postprocessing console (Syngo.Via; Siemens Healthcare GmbH, Erlangen, Germany). One radiologist (R.H.) with 8 years of experience

**TABLE 1.** Demographic and Clinical Characteristics of the Study Participants

Characteristics	Participants (n = 46)
Mean age	66 $\pm$ 11
Mean weight, kg	77.9 $\pm$ 19.9
Mean height, cm	171.6 $\pm$ 10.3
Sex, n (%)	
Female	26 (57)
Male	20 (43)
Race or ethnic group, n (%)	
Mixed, other	2 (4)
White	44 (96)
Disease	
Lung cancer	9 (20)
Cancer other primary	35 (76)
(Post)infectious	2 (4)
Examination status	
Protocol completed	45 (98)
Technical difficulties	1 (2)
Measurement aborted	0

Note: Data in parentheses are percentages. Plus-minus values are means  $\pm$  SD.

in cross-sectional imaging analyzed the blinded data in a 2-step analysis. Each lung nodule's longest and orthogonal diameters were measured to 1 decimal place in the transverse plane of the MRI acquisitions. The radiologist matched the lesions with those in the coronal planes to avoid false-positive detection of lung nodules. Only lung nodules were evaluated; other lung lesions such as consolidation, atelectasis, reticulation, and pleural lesions were not included. During the evaluation, the reader was blinded to the study design, personal and clinical information, as well as all other examinations of the participants. The blinded CT images were evaluated in a second reading cycle after 6 weeks (to avoid recall bias) using computer-assisted 3D multiplanar reformations and maximum intensity projections. To improve the detection rate in the CT data set, all images underwent computer-aided detection (syngo.CT Lung CAD; Siemens Healthcare GmbH, Erlangen, Germany) as an additional evaluation.<sup>24–26</sup> The mean diameter of each nodule was calculated to 1 decimal place according to the Lung Imaging Reporting and Data System (Lung-RADS) v. 1.1.<sup>22</sup>

Finally, MRI and CT lung nodule detection results were compared 1-to-1 on a dual-monitor workstation. Each nodule found in MRI was matched with the corresponding nodule detected with CT imaging for statistical analysis. In addition, each missed nodule was analyzed whether the nodule is retrospectively visible in MRI in direct image comparison to CT.

## Statistical Analysis

Statistical analysis was performed using the STATA 17.0 software package (StataCorp, College Station, TX, USA). Mann-Whitney

*U* test was used to compare nominal variables. Nodules missed by the radiologist during the blinded analysis of CT images but detected on MRI were measured in the CT images retrospectively and counted as nodules for the statistical analysis. False-positive MRI results were reported separately. The detection rate was calculated for the whole data set and for the following subgroups: <4 mm, ≥4–<6 mm, ≥6–<8 mm, ≥8–<15 mm, and ≥15 mm. The accuracy of MRI was defined as the ratio of nodules detected on MRI to those detected on CT.

The study design did not allow for calculation of specificity or negative predictive value. The Shapiro-Wilk *W* test was performed to evaluate whether the data for lung nodules per patient and CT and MRI size measurements were normally distributed; in our data set, normal distribution could not be assumed. Spearman rank correlation coefficient was applied to test the correlation between mean nodule dimensions of CT and MRI. Bland-Altman analysis was performed to visualize the agreement between the results of MRI and CT. Adjusted *P* values are reported. A *P* value of less than 0.05 was considered to indicate statistical significance in all analyses.

## RESULTS

A total of 210 consecutive patients with lung nodules scheduled for chest CT were screened, 164 of whom were excluded from study participation. Appointment scheduling issues prevented study participation for 72 patients, 50 patients did not respond to our invitations, 30 patients were not interested, 8 patients had MRI contraindications,

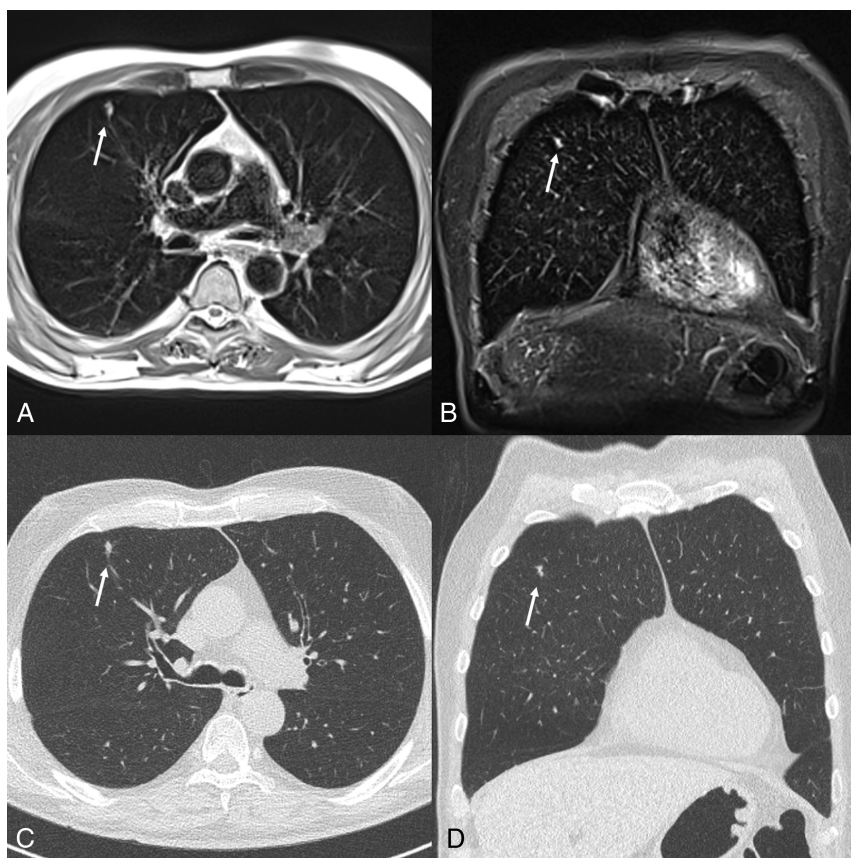


**FIGURE 2.** A 63-year-old patient who underwent PET/CT for staging of diffuse large B-cell lymphoma. Incidental lung nodules were detected, and a follow-up examination was planned. The patient underwent low-field MRI at 0.55 T and CT on the same day. The MRI shows a lung nodule with a size of 7.7 × 4.4 mm in the right upper lobe (arrow) in (A) proton density-weighted sequence with periodically rotated overlapping parallel lines with enhanced reconstruction (PROPELLER) and (B) T2-weighted sequence with short-tau inversion recovery (STIR) preparation and a half-Fourier acquired single-shot turbo spin-echo (HASTE) readout. C and D, Images show the same nodule on CT imaging with 1-mm slice thickness performed on the same day. Because of the small and constant size, additional follow-up was suggested; after growth, resection was performed. Histology revealed a 1.1-cm pT1b non-small cell lung carcinoma.

and 4 patients died before the examination. Ultimately, lung MRI was performed on a total of 46 participants (mean age  $\pm$  SD,  $61 \pm 11$  years; 26 women; Fig. 1). The characteristics of the participants are presented in Table 1.

## Lesion Detection

A total of 964 nodules measuring 0.9 to 27.5 mm (mean diameter,  $4.1 \pm 3.0$  mm) were identified in 46 CT examinations. Every patient had at least 1 nodule, and the average number of lesions per patient was 21. Figures 2 to 4 and Supplemental Digital Content, Figures S1 <http://links.lww.com/RLI/A835> and S2, <http://links.lww.com/RLI/A836>, show examples of representative lung nodules.

Magnetic resonance imaging correctly identified 432 nodules and failed to identify 532, resulting in an overall accuracy of 44.8%. In our study, every nodule with a size of  $\geq 6$  mm detected with CT was detected with MRI (126 nodules, accuracy 100%). The smallest nodule detected with MRI had a diameter of 1.5 mm, and the largest had a diameter of 27.5 mm. In total, 326 nodules had a diameter  $\geq 4$  mm, and 285 (87.4%) of these were correctly identified in MRI. Among nodules with a diameter  $< 3$  mm, 45 of 371 (12.1%) were detected on MRI. Figure 5 shows an example of a detected micronodule. The mean diameter of nodules detected by MRI was  $5.8 \pm 3.8$  mm, which was larger ( $P < 0.001$ ) than the mean diameter of those missed in MRI ( $2.8 \pm 0.8$  mm).

Nodules missed in MRI had a diameter of 0.9 to 5.8 mm. Two thirds (66.9%) of the 532 missed lesions had a diameter  $\leq 3$  mm (356). The distribution of the other missed lesions was as follows: 25.9% (138/532) were  $> 3 \text{--} 4$  mm, 6.2% (33/532) were  $> 4 \text{--} 5$  mm, and under 1% (5/532) were

$> 5 \text{--} 6$  mm. The detection accuracy within size-based subgroups is presented in Table 2.

In total, there were 5/432 (1%) false-positive nodules in MRI; their mean size was  $6.7 \pm 4.3$  mm (range, 3.9–14.2 mm). In comparison to the CT images, 1 lesion was found to have no anatomic correlate, 3 turned out to be pulmonary scars, and 1 was a vessel ectasia.

Eight ground-glass nodules with a mean diameter of  $3.9 \pm 1.7$  mm were detected on CT, with an accuracy of 25% (2/8) for MRI, and 8 partial solid nodules with a mean diameter of  $9.0 \pm 3.5$  mm were detected with an accuracy of 100%.

Seven nodules with a mean diameter of  $3.7 \pm 2.3$  mm were detected on MRI, but missed by the radiologist and the computer-aided detection on CT.

In direct comparison of MR and CT images, 46 additional nodules ( $3.4 \pm 0.8$  mm) were visible in MRI, which were significantly larger ( $P < 0.001$ ) than still not visible ones ( $n = 486$ ,  $2.8 \pm 0.8$  mm). Table 2 shows the detection rates of direct comparison. In 20 cases, potential reasons for missed detection were identified (9 subpleural location, 5 adjacent nodules, 4 perifissural location, 1 masked by consolidation, 1 only visible in transversal plane). Supplemental Digital Content Figures S3 <http://links.lww.com/RLI/A837>, S4 <http://links.lww.com/RLI/A838>, S5 <http://links.lww.com/RLI/A841> to S6 <http://links.lww.com/RLI/A842> show examples of missed nodules.

## Nodule Size Measurement

There were 432 nodules detected by both MRI and CT, with a strong positive correlation between the mean nodule diameter measured

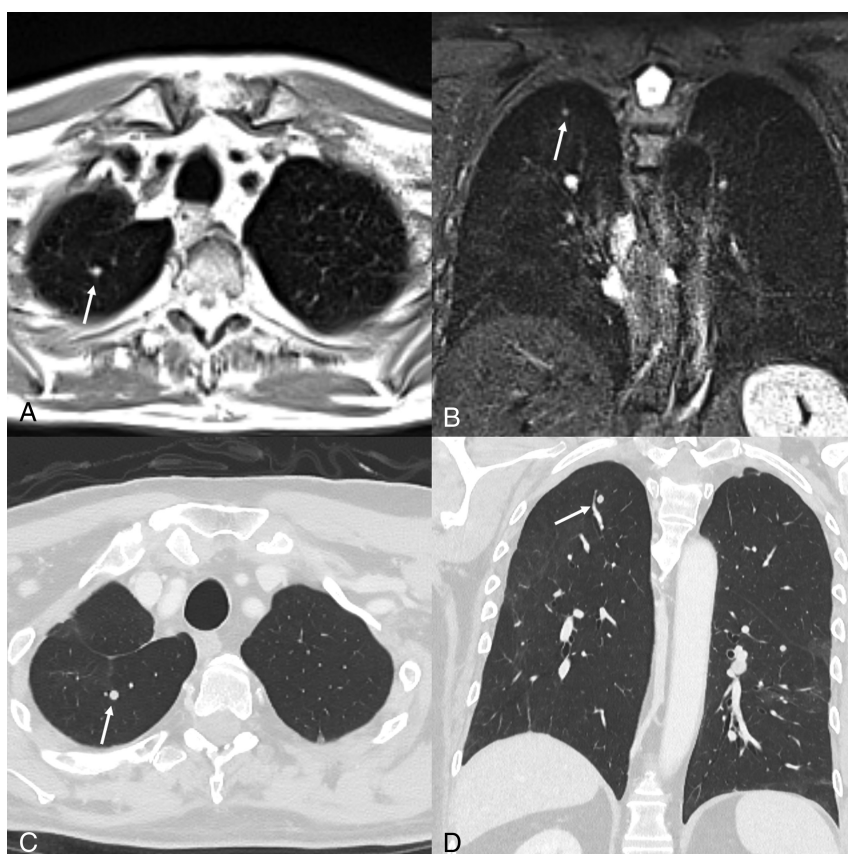


**FIGURE 3.** A 77-year-old patient with malignant melanoma underwent lung MRI at 0.55 T and CT imaging. Both modalities show a  $5.2 \times 4.3$ -mm lung nodule in the right upper lobe (arrow) in (A) proton density-weighted sequence with periodically rotated overlapping parallel lines with enhanced reconstruction (PROPELLER) and (B) T2-weighted sequence with short-tau inversion recovery (STIR) preparation and a half-Fourier acquired single-shot turbo spin-echo (HASTE) readout. C and D, Images show the same nodule on CT imaging with 1.0-mm slice thickness performed on the same day.

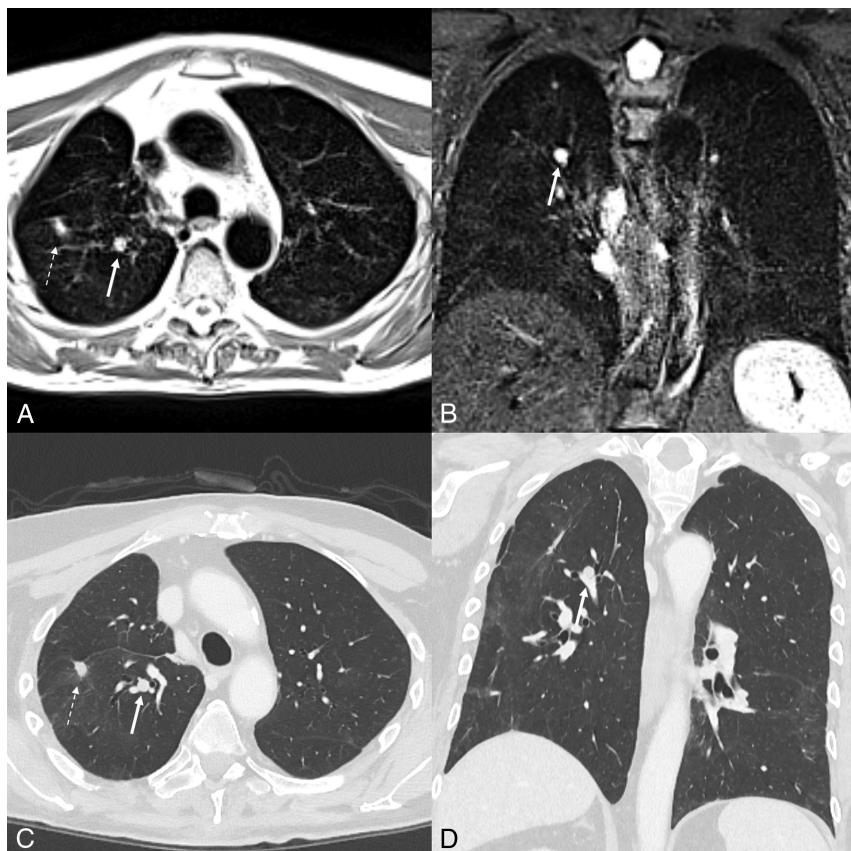


**FIGURE 4.** Metastasis of malignant melanoma ( $8.5 \times 8.2$  mm; arrow) in a 77-year-old patient. Both transversal proton density-weighted periodically rotated overlapping parallel lines with enhanced reconstruction (PROPELLER) imaging (A) and coronal T2-weighted short-tau inversion recovery (STIR) preparation with a half-Fourier acquired single-shot turbo spin-echo (HASTE) readout (B) clearly visualize the nodule. In contrast, the lesion was difficult to detect in transversal (C) and coronal (D) CT imaging because of its proximity to the vessels around it. The axial planes show a partial volume of another metastasis ( $12.4 \times 8.8$  mm; dashed arrow).

Downloaded from <http://journals.lww.com/investigativeradiology> by BhDMf5ePHKav1ZEoum1tQfMa+JLHfZg on 09/01/2023

in MRI and CT images ( $r = 0.87$ ,  $P < 0.001$ ). The Bland-Altman plot visually demonstrates a high agreement between the mean diameter measured in CT and MRI, with a mean difference of  $0.16 \pm 0.9$  mm (Fig. 6).

## DISCUSSION

Lung nodule detection is primarily reserved for CT imaging, which requires radiation exposure. This study aimed to answer whether modern low-field MRI of the lung at 0.55 T could be an alternative to CT imaging for detecting and measuring clinically relevant lung nodules. Therefore, we compared 964 lung nodules in 46 participants in a prospective study design with blinded evaluation. Our study demonstrated a high accuracy for nodule detection, with a detection rate of 80% for nodules ranging from  $\geq 4$  to  $< 6$  mm (159/200) and a 100% detection rate for nodules  $\geq 6$  mm (126/126). Most lesions missed in MRI had a diameter smaller than 3 mm (356/532). Size analysis revealed a very strong correlation between MRI and CT measurements ( $r = 0.87$ ,  $P < 0.001$ ), with a mean difference of  $0.16 \pm 0.9$  mm.

The limited image quality of lung MRI, as well as its physical challenges, low availability, high cost, and physical status requirements for patients, has resulted in its remaining a niche method, with its only clinical use being the surveillance of cystic fibrosis in children.<sup>11,12,18,27</sup> Chest CT remains the reference for lung imaging, as its spatial resolution and short acquisition time are unattainable with other methods. However, chest CT requires a not inconsiderable radiation dose. Therefore, vulnerable patient groups often undergo x-ray, although its sensitivity and specificity

for lesion detection and characterization are lower than achieved with CT and MRI.<sup>28</sup> In recent years, technical improvements have led to better image quality with low-field MRI. Several studies reported the potential of modern low-field MRI for the detection and surveillance of chronic lung disease, pulmonary hypertension, and infection.<sup>17,20,27,29</sup> Patient groups with a high vulnerability to radiation, such as children and pregnant women, can particularly benefit from these techniques. Moreover, MRI can not only provide structural imaging, but also add dedicated tissue information to differentiate between benign and malignant lesions and allow functional analysis of lung ventilation and perfusion.<sup>8–10,30</sup> Recent results showed that lung MRI could provide structural and functional surveillance in adults and children after SARS-CoV-2 infection.<sup>13,20,21,31</sup>

One of the most relevant tasks in chest imaging is the early detection of potential malignancies of the lung due to the high mortality of lung cancer in advanced stages and its significant burden on society and the health care system.<sup>2,32,33</sup> High spatial resolution is necessary to detect and characterize pulmonary nodules correctly.<sup>12</sup> Low-field MRI has intrinsic physical benefits, such as reduced susceptibility artifacts, and emerging scanner techniques enable accurate respiratory-gated imaging, resulting in motion artifact reduction.<sup>16,34</sup>

First results obtained with lung MRI at 0.55 T emphasize the potential for reliable detection of lung nodules. Campbell-Washburn et al<sup>19</sup> reported an excellent lung nodule detection rate in an investigational trial of low-field MRI at 0.55 T that included 24 patients with different lung abnormalities. However, only 14 nodules  $\geq 4$  mm were detected in this heterogeneous study cohort, indicating the need for further research

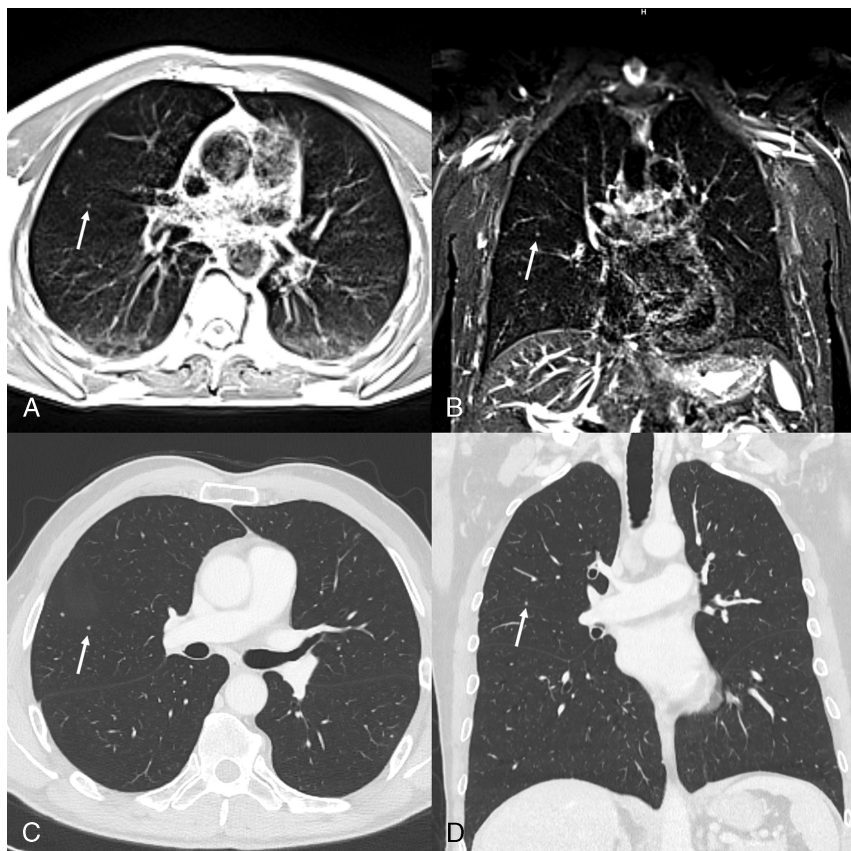


**FIGURE 5.** Perifissural micronodule with a size of  $2.5 \times 2.1$  mm in the right upper lobe in a 55-year-old patient with rectum carcinoma. The MRI shows good image quality of proton density-weighted sequence with periodically rotated overlapping parallel lines with enhanced reconstruction (PROPELLER) (A) and with T2-weighted sequence with short-tau inversion recovery (STIR) preparation and a half-Fourier acquired single-shot turbo spin-echo (HASTE) readout (B) compared with corresponding CT images (C and D).

Downloaded from http://journals.lww.com/investigativeradiology by BhDMf5ePHKav1zEoum1QfMa+KuLhZgb on 09/01/2023

on this promising topic. In our study, we attempted to extend these initial results to a larger group of participants and lung nodules. Moreover, we tried to improve the imaging parameters and reduce motion-related artifacts by implementing a proton density-weighted transversal PROPELLER sequence.

In addition to the physical shortcomings at higher magnetic field strengths, high rates of false-positive results were reported in previous studies at 1.5 T.<sup>35–37</sup> One study comparing CT and different sequences at 1.5 T MRI with a total of 114 lung lesions reported a number of false-positive lesions, ranging from 1 to 48 per sequence (mean 17 per sequence).<sup>35</sup> To reduce the rate of false-positive findings, we added a coronal T2-weighted HASTE sequence and correlated each nodule on both planes during the analysis of MR images. This approach resulted in a small number of false-positive results in our study (5/437, 1%), with 4 of these being misinterpreted scars or ectatic vessels. Only one small

lesion had no structural correlate (1/437, <1%). Our results also revealed an excellent accuracy for clinically relevant nodules with a size of  $\geq 6$  mm (126/126, 100%). Likely benign lung nodules with a size of  $\geq 4$ – $<6$  mm were detected at a rate of 80% (159/200).<sup>7,22</sup> Comparing these results to previous trials at higher field strength, our evaluation suggests that low-field MRI might be a valuable tool in lung cancer screening. A recent study using 1.5 T lung MRI showed that it could be used in a screening setting according to Lung-RADS without missing any lung cancer in the study population. The detection rate reported in the study was 40/41 (98%) for solid nodules of  $\geq 6$  mm and 62/89 (70%) for nodules of  $\geq 4$ – $<6$  mm,<sup>36</sup> which was outperformed by our approach. However, further studies with large screening cohorts are needed to evaluate the role of low-field MRI for lung cancer screening programs. A potential issue for lung cancer screening with MRI might be small but aggressive partial solid nodules, which could be missed by

**TABLE 2.** Detected Lung Nodules

Mean Nodule Diameter	<4 mm	$\geq 4$ – $<6$ mm	$\geq 6$ – $<8$ mm	$\geq 8$ – $<15$ mm	$\geq 15$ mm
No. lesions	638	200	67	39	20
Lesions detected primary on MRI (%)	23% (147/638)	80% (159/200)	100% (67/67)	100% (39/39)	100% (20/20)
Lesions detected in direct comparison of MRI and CT (%)	29% (184/638)	84% (168/200)	100% (67/67)	100% (39/39)	100% (20/20)
Risk of malignancy*	<1%	<1%	1%–2%	10%–15%	>15%

\*According to Lung Imaging Reporting and Data System (Lung-RADS) v. 1.1 for solid nodules.<sup>22</sup>

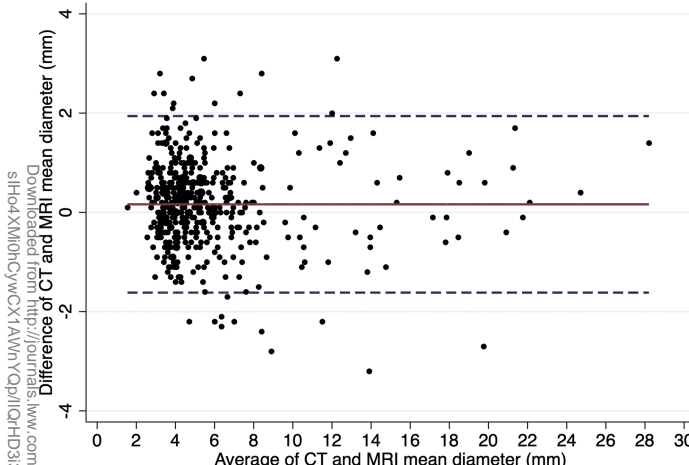


**FIGURE 6.** Bland-Altman plot showing the agreement of mean nodule diameter between CT and MRI. The mean difference between MRI and CT was 0.16 mm (red line); 23/432 nodules are outside the agreement limits (5.3%). The 95% limits of agreement are between -1.62 mm and 1.94 mm (dashed blue lines), and the mean CT and MRI diameter ranges from 1.55 mm to 28.2 mm.

MRI, potentially resulting in a missed opportunity for timely follow-up examination.

Our study had several limitations. First, we had a small group of participants with different underlying diseases and a strong selection bias due to the presence of lung nodules in every participant. We were not able to include healthy controls for ethical reasons, which precluded the calculation of specificity. For organizational reasons, we were also unable to include patients with lung CTs without lung nodules, because of the time delay between reading and the potential inclusion for MRI at the same day. The pretest probability of 100% for lung nodules within our study cohort could have influenced the accuracy rates. Second, we cannot provide a comparison to other field strengths or any histological information of the detected nodules. We are aware that different etiologies could influence the intensity of MR images. Third, image evaluation was only performed by 1 reader. However, previous data suggest that using computer-aided detection analysis as a second reader in lung nodule detection is superior to conventional double reading.<sup>25</sup> A further limitation is the small number of partial solid and ground glass nodules. Size measurement of lung nodules was performed separately in MRI and CT, which may cause deviating definitions of long and short axis of lung nodules.<sup>38</sup> In addition, lower resolution may affect the appearance of lung nodules in MRI, which may also lead to differences in size measurement. A further limitation with potential negative impact on image quality is the much longer acquisition times in MRI compared with CT.

To our knowledge, we performed the first feasibility study of lung nodule detection according to Lung-RADS on a modern low-field MRI with a transversal proton density-weighted periodically rotated overlapping PROPELLER sequence in combination with a coronal T2-weighted HASTE sequence. This approach provided a high accuracy for detection of lung nodules  $\geq 4$  mm, an excellent accuracy for those  $\geq 6$  mm, and a very strong correlation between nodule diameters measured in low-field MRI and CT imaging in a sample of 46 patients. In contrast, MRI was not able to compete with CT in the detection of small nodules. The results suggest that low-field lung MRI could be an alternative to CT for detecting lung metastasis, especially in vulnerable patient populations or if repeated lung examinations are anticipated. Thus, lung MRI at 0.55 T is a promising option for future lung cancer screening programs. Therefore, additional research in screening population is needed.

## ACKNOWLEDGMENTS

The authors thank the Imaging Science Institute Erlangen for providing us with measurement time and technical support. Many thanks to Sandy Schmidt for the technical assistance during MRI.

The present work was performed in (partial) fulfillment of the requirements for obtaining the degree "Dr. med." for M.H.

## REFERENCES

- Huda W, He W. Estimating cancer risks to adults undergoing body CT examinations. *Radiat Prot Dosimetry*. 2012;150:168–179.
- National Lung Screening Trial Research Team, Aberle DR, Adams AM, Berg CD, et al. Reduced lung-cancer mortality with low-dose computed tomographic screening. *N Engl J Med*. 2011;365:395–409.
- de Koning HJ, van der Aalst CM, de Jong PA, et al. Reduced lung-cancer mortality with volume CT screening in a randomized trial. *N Engl J Med*. 2020;382:503–513.
- Leiter U, Buettner PG, Eigenthaler TK, et al. Is detection of melanoma metastasis during surveillance in an early phase of development associated with a survival benefit? *Melanoma Res*. 2010;20:240–246.
- Becker N, Motsch E, Trotter A, et al. Lung cancer mortality reduction by LDCT screening—results from the randomized German LUSI trial. *Int J Cancer*. 2020;146:1503–1513.
- Leleu O, Basille D, Auquier M, et al. Results of second round lung cancer screening by low-dose CT scan—French cohort study (DEP-KP80). *Clin Lung Cancer*. 2022;23:e54–e59.
- Kastner J, Hossain R, Jeudy J, et al. Lung-RADS version 1.0 versus lung-RADS version 1.1: comparison of categories using nodules from the National Lung Screening Trial. *Radiology*. 2021;300:199–206.
- Hausmann D, Jochum S, Utikal J, et al. Comparison of the diagnostic accuracy of whole-body MRI and whole-body CT in stage III/IV malignant melanoma. *J Dtsch Dermatol Ges*. 2011;9:212–222.
- Li B, Li Q, Chen C, et al. A systematic review and meta-analysis of the accuracy of diffusion-weighted MRI in the detection of malignant pulmonary nodules and masses. *Acad Radiol*. 2014;21:21–29.
- Liu J, Yang X, Li F, et al. Preliminary study of whole-body diffusion-weighted imaging in detecting pulmonary metastatic lesions from clear cell renal cell carcinoma comparison with CT. *Acta Radiol*. 2011;52:954–963.
- Hatabu H, Ohno Y, Gefter WB, et al. Expanding applications of pulmonary MRI in the clinical evaluation of lung disorders: Fleischner society position paper. *Radiology*. 2020;297:286–301.
- Wielputz MO. MRI of pulmonary nodules: closing the gap on CT. *Radiology*. 2022;302:707–708.
- Lévy S, Heiss R, Grimm R, et al. Free-breathing low-field MRI of the lungs detects functional alterations associated with persistent symptoms after COVID-19 infection. *Invest Radiol*. 2022;57:742–751.
- Bhattacharya I, Ramasawmy R, Javed A, et al. Assessment of lung structure and regional function using 0.55 T MRI in patients with lymphangioleiomyomatosis. *Invest Radiol*. 2022;57:178–186.
- Wieslander B, Seemann F, Javed A, et al. Impact of vasodilation on oxygen-enhanced functional lung MRI at 0.55 T. *Invest Radiol*. 2023.
- Campbell-Washburn AE, Ramasawmy R, Restivo MC, et al. Opportunities in interventional and diagnostic imaging by using high-performance low-field-strength MRI. *Radiology*. 2019;293:384–393.
- Heiss R, Nagel AM, Laun FB, et al. Low-field magnetic resonance imaging: a new generation of breakthrough technology in clinical imaging. *Invest Radiol*. 2021;56:726–733.
- Campbell-Washburn AE. 2019 American Thoracic Society BEAR cage winning proposal: lung imaging using high-performance low-field magnetic resonance imaging. *Am J Respir Crit Care Med*. 2020;201:1333–1336.
- Campbell-Washburn AE, Malayeri AA, Jones EC, et al. T2-weighted lung imaging using a 0.55-T MRI system. *Radiol Cardiothorac Imaging*. 2021;3:e200611.
- Heiss R, Grodzki DM, Horger W, et al. High-performance low-field MRI enables visualization of persistent pulmonary damage after COVID-19. *Magn Reson Imaging*. 2021;76:49–51.
- Heiss R, Tan L, Schmidt S, et al. Pulmonary dysfunction after pediatric COVID-19. *Radiology* 2022;306:e221250.
- Lung-RADS® Version 1.1. American College of Radiology. Available at: <https://www.acr.org/-/media/ACR/Files/RADS/Lung-RADS/LungRADSAssessmentCategoriesv1-1.pdf>. Accessed June 30, 2023.
- Pinsky PF, Gierada DS, Black W, et al. Performance of lung-RADS in the National Lung Screening Trial: a retrospective assessment. *Ann Intern Med*. 2015;162:485–491.

24. Das M, Mühlenbruch G, Mahnken AH, et al. Small pulmonary nodules: effect of two computer-aided detection systems on radiologist performance. *Radiology*. 2006;241:564–571.
25. Rubin GD, Lyo JK, Paik DS, et al. Pulmonary nodules on multi-detector row CT scans: performance comparison of radiologists and computer-aided detection. *Radiology*. 2005;234:274–283.
26. Zhao Y, de Bock GH, Vliegenthart R, et al. Performance of computer-aided detection of pulmonary nodules in low-dose CT: comparison with double reading by nodule volume. *Eur Radiol*. 2012;22:2076–2084.
27. Wielpütz MO, von Stackelberg O, Stahl M, et al. Multicentre standardisation of chest MRI as radiation-free outcome measure of lung disease in young children with cystic fibrosis. *J Cyst Fibros*. 2018;17:518–527.
28. Sodhi KS, Sharma M, Saxena AK, et al. MRI in thoracic tuberculosis of children. *Indian J Pediatr*. 2017;84:670–676.
29. Anjorin A, Schmidt H, Posselt HG, et al. Comparative evaluation of chest radiography, low-field MRI, the Shwachman-Kulczycki score and pulmonary function tests in patients with cystic fibrosis. *Eur Radiol*. 2008;18:1153–1161.
30. Fink C, Puderbach M, Bock M, et al. Regional lung perfusion: assessment with partially parallel three-dimensional MR imaging. *Radiology*. 2004;231:175–184.
31. Campbell-Washburn AE, Suffredini AF, Chen MY. High-performance 0.55-T lung MRI in patient with COVID-19 infection. *Radiology*. 2021;299:E246–e7.
32. Mariotto AB, Enewold L, Zhao J, et al. Medical care costs associated with cancer survivorship in the United States. *Cancer Epidemiol Biomarkers Prev*. 2020;29:1304–1312.
33. Global Burden of Disease 2019 Cancer Collaboration, Kocarnik JM, Compton K, Dean FE, et al. Cancer incidence, mortality, years of life lost, years lived with disability, and disability-adjusted life years for 29 cancer groups from 2010 to 2019: a systematic analysis for the global burden of disease study 2019. *JAMA Oncol*. 2022;8:420–444.
34. Meier-Schroers M, Kukuk G, Homsi R, et al. MRI of the lung using the PROPELLER technique: artifact reduction, better image quality and improved nodule detection. *Eur J Radiol*. 2016;85:707–713.
35. Cieszanowski A, Lisowska A, Dabrowska M, et al. MR imaging of pulmonary nodules: detection rate and accuracy of size estimation in comparison to computed tomography. *PloS One*. 2016;11:e0156272.
36. Meier-Schroers M, Homsi R, Gieseke J, et al. Lung cancer screening with MRI: evaluation of MRI for lung cancer screening by comparison of LDCT- and MRI-derived lung-RADS categories in the first two screening rounds. *Eur Radiol*. 2019;29:898–905.
37. Meier-Schroers M, Homsi R, Schild HH, et al. Lung cancer screening with MRI: characterization of nodules with different non-enhanced MRI sequences. *Acta Radiol*. 2019;60:168–176.
38. Han D, Heuvelmans MA, Vliegenthart R, et al. Influence of lung nodule margin on volume- and diameter-based reader variability in CT lung cancer screening. *Br J Radiol*. 2018;91:20170405.